JOURNAL OF COMPUTATIONAL PHYSICS **145,** 743–757 (1998)
ARTICLE NO. CP986052

Spectral Collocation on Triangular Elements

Wilhelm Heinrichs

Universität GH Essen, Ingenieurmathematik (FB 10) Universitätsstr. 3, D-45117 Essen, Germany
E-mail: heinrich@ing.math.uni-essen.de

Received December 2, 1997; revised June 23, 1998

We consider the Poisson problem on a segment of the unit disc and on triangles. On the segment we transform the Poisson problem by means of polar coordinates. In these new coordinates we have a problem in a rectangle which can easily be mapped onto the square. Here standard Chebyshev collocation techniques can be applied. Then the segment is mapped onto a triangle where the same spectral scheme may be used. By numerical tests we observed the expected high spectral accuracy. Due to the corner singularity a singular behaviour of the solution can be expected. Here we improved the accuracy by auxiliary mapping techniques. Further, it is shown that finite difference preconditioning can be successfully applied in order to construct an efficient iterative solver. Finally, a domain decomposition technique is applied to the patching of a rectangular and a triangular element.

Key Words: spectral; collocation; triangles; auxiliary mapping; preconditioning; domain decomposition.

1. INTRODUCTION

It is well known that spectral collocation schemes can be successfully applied to elliptic problems in rectangular domains. For smooth solutions the high (exponential) spectral accuracy can be achieved. Here we are interested in spectral collocation on triangular elements. For the p- and the h-p-version of the finite element method the optimal nodes for quadrature are investigated by Babuška *et al.* [1, 3–5]. These techniques are limited to finite element discretizations. For spectral schemes it is not a priori clear which collocation nodes have to be chosen. It is not possible to employ the standard Gauss–Lobatto nodes in both directions. Hesthaven [12] presented optimal nodal sets based on an electrostatic interpretation of the nodes. Gottlieb and Hesthaven [9] studied stable spectral schemes for conservation laws on triangles with unstructured grids. Sherwin and Karniadakis [14] proposed an unstructured spectral element method on triangular and tetrahedral subdomains, where a special spectral basis (see Dubiner [7]) has been employed. Wingate *et al.* [15–17] consider spectral element methods on triangles for geophysical fluid dynamics problems

0021-9991/98 $25.00

and the shallow water equations. Here special function spaces for triangular spectral elements are introduced. Modifications of the classical modified Dubiner's basis are proposed, called an "interior-orthogonal" basis. The new basis retains the most important properties of the Dubiner's basis, but gives a weight matrix which is simpler. Here we follow a completely different approach where the standard spectral Cheyshev basis is used. We propose a mapping technique where the Poisson problem is first mapped onto a segment of the unit disc. For this purpose polar coordinates are used. In polar coordinates we have a rectangular domain in $(r, \theta) \in \Omega_{\theta_1} = (0, 1) \times (0, \theta_1)$ for $0 < \theta_1 \leq 2\pi$. Then for $0 < \theta_1 < \pi$ the circular boundary of the segment is mapped onto an edge of the triangle. This means that now r depends on θ, i.e., $r = r(\theta)$. In Ω_{θ_1} we discretize by means of the standard Chebyshev collocation scheme. Hence we approximate by Chebyshev polynomials and collocation is performed at the Chebyshev Gauss–Lobatto nodes in (r, θ). Homogeneous Dirichlet boundary conditions are enforced on the boundary $\partial\Omega_{\theta_1}$. It is numerically shown that for smooth solutions the high spectral accuracy can be achieved. However, the geometric singularity often gives rise to singular solutions. Here we investigated auxiliary mapping techniques to smooth the singularity. This approach was intensively studied by Pathria and Karniadakis [13] for spectral elements. The problem is mapped from Ω_{θ_1} to Ω_π so that the corner is eliminated. But now the singularity is caused by the singular behaviour of the right-hand side. Nevertheless for $\theta_1 > \pi/\sqrt{2}$ the singularity is now much weaker, which leads to an improvement in accuracy. This is confirmed by numerical experiments. Finally we study finite difference preconditioning. It is shown that the condition number becomes independent of N. This can be used in constructing efficient iterative solvers. For more complicated geometries, where rectangular and triangular subdomains match, we propose a domain decomposition technique. Here a Dirichlet–Neumann interface relaxation (see Funaro, Quarteroni, and Zanolli [8]) is iterated until continuity of normal derivatives is achieved. Numerical results demonstrate the efficiency of our treatment.

2. TRANSFORMATION OF TRIANGULAR ELEMENTS

We consider the Poisson problem in a segment, i.e.,

$$\Delta u = f \quad \text{in } \Omega_{\theta_1}, \tag{1}$$

$$u = 0 \quad \text{on } \partial\Omega_{\theta_1}, \tag{2}$$

where f denotes a given force and

$$\Omega_{\theta_1} = \{(x, y) = r(\cos\theta, \sin\theta) : 0 < r < 1, 0 < \theta < \theta_1\}$$

denotes a segment with angle θ_1. As usual $\partial\Omega_{\theta_1}$ denotes the boundary of Ω_{θ_1}. In polar coordinates the Poisson problem can equivalently be written as

$$r^2 u_{rr} + r u_r + u_{\theta\theta} = r^2 f \quad \text{in } Q_{\theta_1}, \tag{3}$$

$$u = 0 \qquad \text{on } \partial Q_{\theta_1}, \tag{4}$$

where

$$Q_{\theta_1} = \{(r, \theta) : 0 < r < 1, 0 < \theta < \theta_1\}.$$

Here we multiplied the transformed Laplace operator by r^2. As we see later this representation has advantages for preconditioning.

Further, we are interested in the Poisson problem on triangular elements given by

$$T_{\theta_1} = \left\{ (x, y) = \frac{r}{\cos\theta + t_1 \sin\theta}(\cos\theta, \sin\theta) : 0 < r < 1, 0 < \theta < \theta_1 \right\},$$

where

$$t_1 = \tan\frac{\theta_1}{2}.$$

T_{θ_1} results from Ω_{θ_1} by mapping the circular boundary to an edge of the triangle. This is accomplished by the mapping

$$r \to r(\theta) = \frac{r}{\cos\theta + t_1 \sin\theta}.$$

Hereby we obtain the third edge which is in (x, y) coordinates, given by

$$x + t_1 y = 1.$$

For instance, for $\theta_1 = \pi/2$ we obtain $t_1 = 1$ and the straight line $y = 1 - x$. For a fixed radius r, $0 < r < 1$, the transform is given by $x + t_1 y = r$ and $\tan\theta = y/x$. This yields

$$u_x = u_r - \frac{y}{x^2 + y^2} u_\theta,$$

$$u_{xx} = u_{rr} - \frac{2y}{x^2 + y^2} u_{r\theta} + \frac{y^2}{(x^2 + y^2)^2} u_{\theta\theta} + \frac{2xy}{(x^2 + y^2)^2} u_\theta$$

and

$$u_y = t_1 u_r + \frac{x}{x^2 + y^2} u_\theta,$$

$$u_{yy} = t_1^2 u_{rr} + 2t_1 \frac{x}{x^2 + y^2} u_{r\theta} + \frac{x^2}{(x^2 + y^2)^2} u_{\theta\theta} - \frac{2xy}{(x^2 + y^2)^2} u_\theta.$$

Hence, the Poisson problem in T_{θ_1} can equivalently be written as

$$\left(1 + t_1^2\right)(x^2 + y^2) u_{rr} + 2(t_1 x - y) u_{r\theta} + u_{\theta\theta} = (x^2 + y^2) f \quad \text{in } T_{\theta_1} \tag{5}$$

$$u = 0 \quad \text{on } \partial T_{\theta_1}, \tag{6}$$

or

$$\frac{1 + t_1^2}{(\cos\theta + t_1 \sin\theta)^2} r^2 u_{rr} + 2\frac{t_1 \cos\theta - \sin\theta}{\cos\theta + t_1 \sin\theta} r u_{r\theta} + u_{\theta\theta} = \frac{r^2}{(\cos\theta + t_1 \sin\theta)^2} f \quad \text{in } Q_{\theta_1}$$

$$u = 0 \quad \text{on } \partial Q_{\theta_1}.$$

Therefore, in both cases we are able to transform the Poisson problem onto the rectangle Q_{θ_1}.

3. SPECTRAL DISCRETIZATION

For the spectral approximation we use a standard Chebyshev collocation scheme. It is defined on the Chebyshev Gauss–Lobatto nodes given by

$$(s_i, t_j) = \left(\cos \frac{i\pi}{N}, \cos \frac{j\pi}{N} \right), \quad i, j = 0, \ldots, N.$$

Hence fast Fourier transforms (FFTs) are available for the efficient evaluation of spectral derivatives. In the two-dimensional case they can be evaluated in $O(N^2 \log N)$ arithmetic operations. These nodes are mapped on $(r, \theta) \in (0, 1) \times (0, \theta_1)$ by the linear transform:

$$r_i = \frac{1}{2}(s_i + 1), \quad \theta_j = \frac{\theta_1}{2}(t_j + 1).$$

By using these nodes in (r, θ) we plot for $N = 16$ the collocation nodes on Ω_{θ_1} for $\theta_1 = \pi/2, \pi, \frac{3}{2}\pi$, and T_{θ_1} for $\theta_1 = \pi/2$ in Figs. 1–4. As expected, the nodes are clustering near the corner $r = 0$. Now we present the Chebyshev collocation scheme in the (r, θ) coordinate system. As usual we employ a Chebyshev approximation $u_N \in \mathbb{P}_N^0$, where

$$\mathbb{P}_N^0 = \{p : p \text{ polynomial of degree } \leq N \text{ in } s, t \text{ vanishing on the boundary}\}.$$

u_N can be written as

$$u_N = \sum_{m,n=0}^{N} a_{m,n} T_m(s) T_n(t), \quad a_{m,n} \in \mathbb{R},$$

where $T_m(s) = \cos m \arccos s$ denotes the mth Chebyshev polynomial. The boundary conditions are automatically fulfilled and we require at the $(N-1)^2$ collocation nodes:

$$\left(r^2 u_{rr} + r u_r + u_{\theta\theta}\right)(r_i, \theta_j) = r_i^2 f(r_i, \theta_j) \quad \text{for } i, j = 1, \ldots, N-1.$$

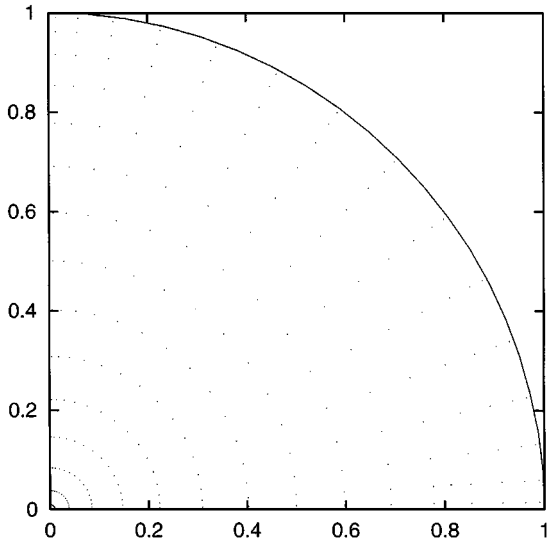

FIG. 1. Collocation nodes in $\Omega_{\pi/2}$.

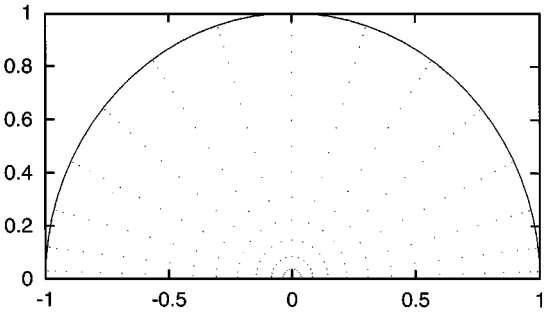

FIG. 2. Collocation nodes in Ω_π.

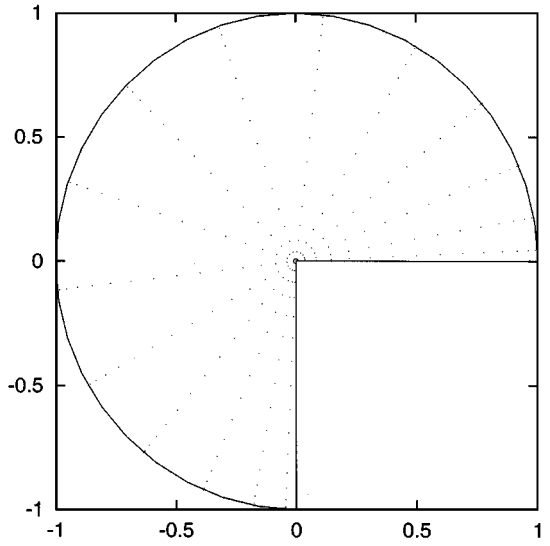

FIG. 3. Collocation nodes in $\Omega_{3\pi/2}$.

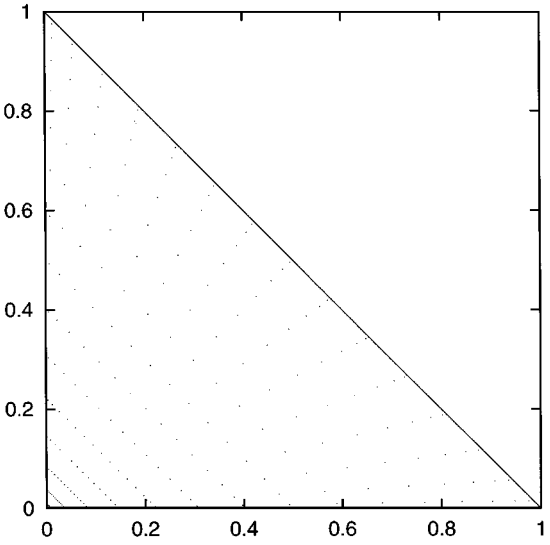

FIG. 4. Collocation nodes in $T_{\pi/2}$.

Similar collocation conditions are required for Eq. (5). The spectral approximation is now uniquely determined. The occurring derivatives $u_{rr}, u_r, u_{\theta\theta}$ can be spectrally evaluated by using the standard Chebyshev collocation derivatives in the (s,t)-coordinate system. Obviously, we obtain

$$u_r = 2u_s, \quad u_{rr} = 4u_{ss},$$
$$u_\theta = \frac{2}{\theta_1}u_t, \quad u_{\theta\theta} = \frac{4}{\theta_1^2}u_{tt}, \quad u_{r\theta} = \frac{4}{\theta_1}u_{st}.$$

The spectral collocation derivative is given by $D_N = (d_{i,j})_{i,j=0,\dots,N}$ (see Canuto *et al.* [2]), where

$$d_{i,j} = \begin{cases} \frac{c_i}{c_j}\frac{(-1)^{i+j}}{s_i - s_j}, & i \neq j, \\ -\frac{s_j}{2(1-s_j^2)}, & 1 \le i = j \le N-1, \\ \frac{2N^2+1}{6}, & i = j = 0, \\ -\frac{2N^2+1}{6}, & i = j = N, \end{cases}$$

and

$$c_i = \begin{cases} 2, & i \in \{0, N\}, \\ 1, & i = 1, \dots, N-1. \end{cases}$$

Partial derivatives can be obtained by means of tensor product representation ($\otimes$) with the identity matrix I_N; i.e.,

$$\frac{\partial}{\partial r} \cong 2(D_N \otimes I_N), \qquad \frac{\partial^2}{\partial r^2} \cong 4\big(D_N^2 \otimes I_N\big),$$
$$\frac{\partial}{\partial \theta} \cong \frac{2}{\theta_1}(I_N \otimes D_N), \quad \frac{\partial^2}{\partial \theta^2} \cong \frac{4}{\theta_1^2}\big(I_N \otimes D_N^2\big),$$
$$\frac{\partial^2}{\partial r\,\partial \theta} \cong \frac{4}{\theta_1}(D_N \otimes D_N).$$

Now the spectral operators are well defined. For these spectral discretizations we expect the high spectral accuracy. For smooth (analytical) solutions exponential convergence can be observed. We tested the accuracy for the following two examples, where the exact solutions (in the (x,y)-coordinate system) are given by

$$u(x,y) = xy\big(e^{x^2+y^2} - e\big), \quad \theta_1 = \pi/2 \tag{7}$$

for problem (3) and

$$u(x,y) = xy(e^{x+y} - e), \quad \theta_1 = \pi/2 \tag{8}$$

for problem (5). We calculated the discrete L^2-error $E2$ which is given by $E2 = \|u - u_N\|$. From the numerical results in Tables I and II, we observe the exponential decay of the error. For example (7), the rounding error accuracy is already reached for $N = 16$. This is due to the fact that the exponent $x^2 + y^2 = r^2$ is independent of θ.

TABLE I
Results for Example (7)

N	$E2$
4	1.94×10^{-3}
8	6.62×10^{-7}
16	7.82×10^{-15}
32	5.79×10^{-15}

From the numerical results we observe a uniform resolution over the whole domain. Clearly, the collocation points are clustering near the corner, but there is nearly no difference in the error distribution. The nodes are optimal since the original problem on the triangular element is transformed onto an elliptic problem on the square. On the square it is well known that Gauss–Lobatto nodes are optimal. A precise convergence analysis is quite difficult because of the singular coefficients in the differential operator. But from the eigenvalue computations in Section 5 it becomes clear that the spectral operator is numerically elliptic.

4. SINGULAR SOLUTIONS AND AUXILIARY MAPPINGS

The geometric singularity (corner in $r = 0$) often gives rise to singular solutions. The irregularity is due to the fact that the differential equation and the boundary conditions are not compatible. This usually leads to a singularity in the corner. The accuracy of the spectral method is then degraded and there is no significant advantage over low-order finite difference or finite element methods. It is possible, however, to use a priori information about the behaviour of the singularity in constructing improved schemes. This has been accomplished by using

- supplementary singular basis functions,
- conformal maps to smooth the singularity,
- domain decomposition techniques or adaptive refinement.

Here we are concerned with auxiliary mappings to smooth the singularity. This technique was already investigated by Pathria and Karniadakis [13] for the spectral element method. For certain simple cases, the problem is transformed to a new coordinate system, where the solution is analytic, and the exponential convergence is recovered. Even when this is not possible, the singularity is usually much weaker after mapping, so that other treatments are more effective in the new coordinate system. Such a singularity occurs if for instance

TABLE II
Results for Example (8)

N	$E2$
4	1.89×10^{-4}
8	8.85×10^{-7}
16	1.84×10^{-11}
32	1.78×10^{-16}

TABLE III
Results for $\theta_1 = \pi/2$

N	*ER*
4	6.30×10^{-5}
8	2.08×10^{-6}
16	4.36×10^{-8}
32	3.81×10^{-10}

$f \equiv -1$; i.e.,

$$-\Delta u = 1 \quad \text{in } \Omega_{\theta_1},$$
$$u = 0 \quad \text{on } \partial\Omega_{\theta_1}.$$

We evaluated u_N in $r = \frac{1}{2}$, $\theta = \theta_1/2$. The computation was performed for $N = 4, 8, 16, 32$ and $\theta_1 = \pi/2, \pi, \frac{3}{2}\pi$. Since the exact solution is not known we compared the values with u_N for $N = 36$. *ER* denotes the error compared to this value. In Tables III, IV, and V we present the numerical results for $\theta_1 = \pi/2, \pi, \frac{3}{2}\pi$.

Only for $\theta_1 = \pi$ do we observe spectral accuracy. In the other two cases there is no exponential convergence, due to the singular behaviour of the solution. For $\theta_1 = \alpha\pi$ it is shown (see [13]) that mapping is recommended for $\alpha > 1/\sqrt{2}$. Hence for $\theta_1 = \frac{3}{2}\pi$ auxiliary mapping leads to improved accuracy. For $\theta_1 = \pi/2$ there is no improvement. The mapping introduces new coordinates

$$\rho = r^{1/\alpha}, \quad \sigma = \frac{\theta}{\alpha} \quad \text{for } \theta_1 = \alpha\pi.$$

Hence, Q_{θ_1} is mapped onto Q_π, where the geometric singularity has disappeared. It is easily seen [13] that Eq. (3) is equivalent to

$$\rho^2 u_{\rho\rho} + \rho u_\rho + u_{\theta\theta} = \alpha^2 \rho^{2\alpha} f \quad \text{in } Q_\pi. \tag{9}$$

Compared to (3) there is only a change in the right-hand side which now leads the singular behaviour. There is no singularity due to geometry. Typical error estimates in the H^1-norm are presented in [13]:

- without mapping,

$$\|u - u_N\| \le C N^{-2/\alpha - \epsilon}, \quad C > 0;$$

TABLE IV
Results for $\theta_1 = \pi$

N	*ER*
4	6.05×10^{-4}
8	3.13×10^{-6}
16	1.01×10^{-9}
32	1.85×10^{-15}

TABLE V
Results for $\theta_1 = \frac{3}{2}\pi$

N	*ER*
4	$1.87 \cdot 10^{-3}$
8	$1.06 \cdot 10^{-4}$
16	$1.37 \cdot 10^{-5}$
32	$6.11 \cdot 10^{-7}$

- with mapping,

$$\|u - u_N\| \leq C N^{-4\alpha-\epsilon}, \quad C > 0$$

for any $\epsilon > 0$. Hence for $\alpha = \frac{3}{2}$ it is recommended to use mapping with an error decay proportional to N^{-6}, instead of $N^{-4/3}$ without mapping. For $\alpha = \frac{1}{2}$ the mapping technique leads to somewhat worse results. Without mapping the error decay is proportional to N^{-4}. These theoretical predictions were fully confirmed by the numerical results presented in the Tables VI and VII.

Finally, we consider a nonsmooth example, where the right-hand side f is discontinuous. We consider Eqs. (3) and (4) with $\theta_1 = \pi/2$. The function f is now defined by

$$f \equiv \begin{cases} -1, & x + y < 1, \\ 0, & x + y \geq 1. \end{cases} \tag{10}$$

Hence, f has a discontinuity along the axes $x + y = 1$. Since now the solution is not smooth, no high accuracy can be expected. From the numerical results in Table VIII it can be observed that a first-order method results. Here no higher accuracy than for finite difference or finite elements can be achieved.

5. PRECONDITIONING

First, we were interested in the eigenspectrum of the first derivative operators. For the standard spectral schemes (see [2]) it is well known that the largest eigenvalues scale as $O(N^2)$. For reasons of symmetry the eigenvalues of $\partial/\partial x$ and $\partial/\partial y$ are the same. On Ω_{θ_1}

TABLE VI
$\theta_1 = \pi/2$ with Mapping

N	*ER*
4	7.54×10^{-4}
8	3.67×10^{-5}
16	2.50×10^{-6}
32	6.36×10^{-8}

TABLE VII
$\theta_1 = \frac{3}{2}\pi$ with Mapping

N	*ER*
4	$8.56 \cdot 10^{-4}$
8	$6.96 \cdot 10^{-6}$
16	$1.47 \cdot 10^{-9}$
32	$1.75 \cdot 10^{-12}$

we obtain

$$u_x = \cos\theta u_r - \frac{\sin\theta}{r} u_\theta,$$
$$u_y = \sin\theta u_r + \frac{\cos\theta}{r} u_\theta.$$

On T_{θ_1} we have

$$u_x = u_r - \frac{\cos\theta + t_1 \sin\theta}{r} \sin\theta u_\theta,$$
$$u_y = t_1 u_r + \frac{\cos\theta + t_1 \sin\theta}{r} \cos\theta u_\theta.$$

We fix $\theta_1 = \pi/2$ and calculate the absolutely maximal eigenvalues $\lambda_{\max}$ for $N = 4, 8, 16, 32$. In Tables IX and X we present the numerical results on Ω_{θ_1}, T_{θ_1} for $\theta_1 = \pi/2$. On Ω_{θ_1} the maximal eigenvalues seem to behave as $O(N^3)$, whereas on T_{θ_1} as $O(N^2)$.

Further we consider finite difference preconditioning for problems (3) and (5). We fix $\theta_1 = \pi/2$. By numerical tests we found that it is better to work with the equations multiplied by r^2. Another good choice for preconditioning is bilinear finite elements, as proposed by Deville and Mund [6]. We have more experience with finite differences. Let w denote a one-dimensional function. The finite difference approximations for the first and second derivative are given by

$$w'(s_j) = 0.5(-\gamma_{j-1} w(s_{j-1}) - (\gamma_j - \gamma_{j-1}) w(s_j) + \gamma_j w(s_{j+1})),$$
$$w''(s_j) = 2\delta_j(\gamma_{j-1} w(s_{j-1}) - (\gamma_j + \gamma_{j-1}) w(s_j) + \gamma_j w(s_{j+1})),$$

TABLE VIII
Results for Example (10)

N	*ER*
4	6.32×10^{-3}
8	1.81×10^{-3}
16	9.56×10^{-4}
32	4.04×10^{-4}

TABLE IX
λ_{max} for $\partial/\partial x$, $\partial/\partial y$ on Ω_{θ_1}, $\theta_1 = \pi/2$

N	λ_{max}	λ_{max}/N^3
4	1.19×10^1	0.19
8	2.01×10^1	0.39
16	3.08×10^3	0.75
32	4.84×10^4	1.48

where

$$\delta_j = \frac{1}{s_{j+1} - s_{j-1}},$$
$$\gamma_j = \frac{1}{s_{j+1} - s_j}, \quad j = 1, \ldots, N-1.$$

The finite difference discretization of Eqs. (3) and (5) can now be derived by tensor product representation. In Tables XI and XII we present the absolute value of the minimal and maximal eigenvalues $\lambda_{\min}$ and $\lambda_{\max}$ for the spectral operators of Eqs. (3) and (5). The quantity

$$\text{cond} = \frac{\lambda_{\max}}{\lambda_{\min}}$$

yields a reasonable approximation of the condition number.

In Tables XIII and XIV we present the corresponding results for the preconditioned spectral operators. As expected, the condition number is dramatically reduced by preconditioning. It is only slightly increasing in N. This is the typical behaviour which was already observed for the spectral Laplacian on rectangular domains (see [10, 11]).

6. DOMAIN DECOMPOSITION

Here we consider the patching of a rectangle with a triangle. We solve the problem

$$\Delta u = f \quad \text{in } \Omega_h, \tag{11}$$
$$u = g \quad \text{on } \partial\Omega_h, \tag{12}$$

TABLE X
λ_{max} for $\partial/\partial x$, $\partial/\partial y$ on T_{θ_1}, $\theta_1 = \pi/2$

N	λ_{max}	λ_{max}/N^2
4	4.00×10^0	0.25
8	1.25×10^1	0.20
16	4.70×10^1	0.18
32	1.83×10^2	0.18

TABLE XI
Results for the Spectral Operator (3)

N	λ_{min}	λ_{max}	Cond
4	4.49	7.59×10^{1}	1.69×10^{1}
8	4.26	1.11×10^{3}	2.59×10^{2}
16	4.16	1.75×10^{4}	4.20×10^{3}
32	4.12	2.79×10^{7}	6.78×10^{6}

TABLE XII
Results for the Spectral Operator (5)

N	λ_{min}	λ_{max}	Cond
4	5.10	1.15×10^{2}	2.26×10^{1}
8	4.58	1.89×10^{3}	4.15×10^{2}
16	4.39	3.07×10^{4}	7.00×10^{3}
32	4.29	4.93×10^{5}	1.15×10^{5}

TABLE XIII
Results for the Preconditioned Operator (3)

N	λ_{min}	λ_{max}	Cond
4	0.63	1.73	2.75
8	0.62	2.13	3.44
16	0.62	2.30	3.73
32	0.62	2.39	3.87

TABLE XIV
Results for the Preconditioned Operator (5)

N	λ_{min}	λ_{max}	Cond
4	0.99	1.71	1.73
8	0.99	2.12	2.13
16	0.80	2.41	3.01
32	0.66	2.83	4.31

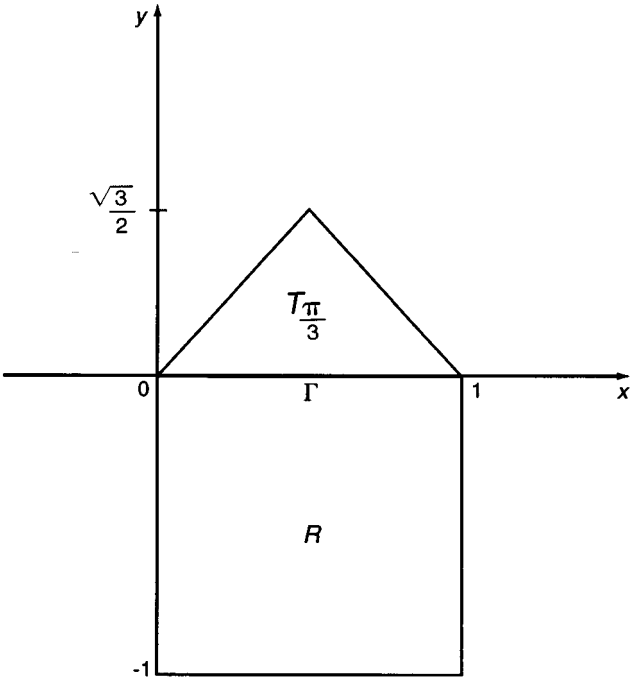

FIG. 5. Shape of Ω_h.

where f and g denote given data and

$$\Omega_h = T_{\theta_1} \cup R, \quad R = (0, 1) \times (-1, 0].$$

We fix $\theta_1 = \pi/3$ so that Ω_h has the shape of a house (see Fig. 5). On the interface $\Gamma = (0, 1)$ we use an interface relaxation procedure as proposed by Funaro, Quarteroni, and Zanolli [8]. Here a sequence of Dirichlet–Neumann problems is iterated until convergence. Continuity of normal derivatives at the interfaces are enforced. The iteration proceeds until C^1 continuity is achieved to some prescribed tolerance (10^{-14} in our experiments). The Poisson problem is solved on each subdomain T_{θ_1} and R. We start with $u_1^0 = u_2^0 \equiv 0$ and then for $m = 1, 2, \ldots$ we iterate as

$$\begin{aligned} \Delta u_1^m &= f && \text{in } T_{\theta_1}, \\ u_1^m &= g && \text{on } \partial T_{\theta_1} - \Gamma, \\ u_1^m &= \delta^m u_2^{m-1} + (1 - \delta^m) u_1^{m-1} && \text{on } \Gamma \end{aligned}$$

and

$$\begin{aligned} \Delta u_2^m &= f && \text{in } R, \\ u_2^m &= g && \text{on } \partial R - \Gamma, \\ \frac{\partial u_2^m}{\partial \nu} &= \frac{\partial u_1^m}{\partial \nu} && \text{on } \Gamma, \ \nu \text{ outer normal}, \end{aligned}$$

where δ^m denotes the relaxation parameter which is chosen dynamically in order to accelerate the convergence. Usually it is the unique real minimizer of the error between successive

TABLE XV
Results for Example (13)

N	It	$E2_1$	$E2_2$
4	11	5.89×10^{-1}	3.80×10^{-1}
8	18	5.49×10^{-3}	3.59×10^{-3}
16	25	5.37×10^{-8}	1.60×10^{-8}
32	36	8.44×10^{-14}	4.95×10^{-14}

iterates and is computed as

$$\delta^m = \frac{\left(e_1^m, e_1^m - e_2^m\right)}{\left\|e_1^m - e_2^m\right\|^2},$$

where $(\cdot, \cdot)$ denotes the discrete L^2 inner product and

$$e_i^m = u_i^m - u_i^{m-1}, \quad i = 1, 2,$$

is the difference between two iterates on the relevant subdomain. This iteration proceeds until some prescribed tolerance along the interface (here 10^{-14}). In Table XV we present the numerical results for an example where the exact solution with nonhomogeneous boundary conditions is given by

$$u(x, y) = \sin\left(3\pi x + \frac{\pi}{4}\right)\sin\left(3\pi y + \frac{\pi}{4}\right), \quad \theta_1 = \frac{\pi}{3}. \tag{13}$$

It denotes the number of interface relaxations which are necessary until convergence. Afterwards the discrete L^2 errors $E2_1, E2_2$ on the subdomains $T_{\pi/3}$ and R are calculated. From the numerical results we once more observe exponential convergence of the patched spectral scheme. Hence, we also found a highly accurate method for domains with five corners. Clearly, these techniques can be generalized to domains with an odd number of corners.

7. SUMMARY

By using polar coordinates, the triangular elements are mapped on rectangular domains, where standard spectral collocation schemes are available. Here a Chebychev collocation method with Gauss–Labatto nodes in the polar coordinates is employed. Both for smooth and singular solutions the expected high spectral accuracy is achieved. The accuracy is determined only by the smoothness of the solution. More complicated geometries consisting of triangular and rectangular subdomains can be treated efficiently by a domain decomposition approach and patching techniques. Here a Dirichlet–Neumann relaxation is iterated until the continuity of the normal derivatives on the interfaces is achieved.

REFERENCES

1. I. Babuška and M. Suri, The p- and h-p version of the finite element method. An overview, *Comput. Methods Appl. Mech. Engrg.* **80**, 5 (1990).
2. C. Canuto, M. Y. Hussaini, A. Quarteroni, and T. A. Zang, *Spectral Methods in Fluid Dynamics*, Series in Computational Physics (Springer-Verlag, Berlin/Heidelberg/New York, 1989).

3. Q. Chen and I. Babuška, Approximate optimal points for polynomial interpolation of a real function in an interval and in a triangle, *Comput. Methods Appl. Mech. Engrg.* **128**, 405 (1996).
4. Q. Chen and I. Babuška, The optimal symmetric points for polynomial interpolation of real functions in the tetrahedron, *Comput. Methods Appl. Mech. Engrg.* **137**, 89 (1996).
5. Q. Chen and I. Babuška, Adaptive procedure for approximating functions by continuous piecewise polynomials, *Comm. Numer. Meth. Engrg.* **12**, 483 (1996).
6. M. Deville and E. Mund, Chebyshev pseudospectral solution of second-order elliptic equations with finite element preconditioning, *J. Comput. Phys.* **60**, 517 (1985).
7. M. Dubiner, Spectral methods on triangular and other domains, *J. Sci. Comput.* **6**, 345 (1991).
8. D. Funaro, A. Quarteroni, and P. Zanolli, An iterative procedure with interface relaxation for domain decomposition methods, *SIAM J. Numer. Anal.* **25**, 1213 (1988).
9. D. Gottlieb and J. S. Hesthaven, Stable spectral methods for conservation laws on triangles with unstructured grids, *SIAM J. Numer. Anal.*, to appear.
10. W. Heinrichs, Line relaxation for spectral multigrid methods, *J. Comput. Phys.* **77**, 166 (1988).
11. W. Heinrichs, Multigrid methods for combined finite difference and Fourier problems, *J. Comput. Phys.* **78**, 424 (1988).
12. J. S. Hesthaven, From electrostatics to almost optimal nodal sets for polynomial interpolation in a simplex, *SIAM J. Numer. Anal.* **35**(2), 655 (1998).
13. D. Pathria and G. E. Karniadakis, Spectral element methods for elliptic problems in nonsmooth domains, *J. Comput. Phys.* **122**, 83 (1995).
14. S. J. Sherwin and G. E. Karniadakis, Triangular and tetrahedral spectral elements, in *Proceedings of the Third International Conference on Spectral and High Order Methods, Houston, Texas, 1996*, edited by A. V. Ilin and L. R. Scott, *Houston J. Math.*
15. B. A. Wingate and J. P. Boyd, Spectral element methods on triangles for geophysical fluid dynamics problems, in *Proceedings of the Third International Conference on Spectral and High Order Methods, Houston, Texas, 1996*, edited by A. V. Ilin and L. R. Scott.
16. B. A. Wingate and M. A. Taylor, The natural function space for triangular spectral elements, *SIAM J. Numer. Anal.*, submitted.
17. B. A. Wingate and M. A. Taylor, A (Fekete) point triangular spectral element method; Application to the shallow water equations, *J. Comput. Phys.*, submitted.